M20100240

A Liquid-Piston Steam Engine

Shinichi Yatsuzuka, Shuzo Oda, Yasunori Niiyama, Kentaro Fukuda and Kazutoshi Nishizawa
DENSO CORPORATION

Naoki Shikazono
THE UNIVERSITY OF TOKYO

ABSTRACT

Recently, waste heat recovery system from automobile exhaust gas has attracted a lot of attention as one of the promising technology to improve fuel efficiency and to reduce carbon dioxide emission. In order to put this system into practice, we developed a novel liquid-piston steam engine which has large potential of high efficiency, high reliability and low cost. Thermal efficiency of 12.7 % is achieved at temperatures of T_h = 270 °C and T_l = 80 °C. Finally, electrical output of waste heat recovery system with the liquid-piston steam engine is estimated to be 44 or 79Wh under NEDC or HWFET modes, respectively.

INTRODUCTION

Waste energy of automobile exhaust gas is as much as 30% of the total fuel energy, which is dissipated to the atmosphere as heat without being used [1]. Waste heat recovery system from automobile exhaust gas that converts exhaust gas energy into kinetic energy or electricity contributes greatly to improve fuel efficiency and to reduce carbon dioxide emission. Waste heat recovery studies have been conducted by most automotive manufacturers. Endo et al. [2] developed a automatically controlled waste heat recovery system using Rankine cycle, and installed it in a hybrid vehicle. It is reported that thermal efficiency was increased from 28.9% to 32.7% at a constant vehicle speed of 100km/h. Ringler et al. [3] investigated various heat recovery technologies and developed a test bench using exhaust gas and coolant based on Rankine cycle. They obtained additional power outputs between 0.7 - 2 kW which corresponds to about 10% improvement of engine performance. However, no waste heat recovery system has been commercialized to date.

In this paper, we introduce a novel liquid-piston steam engine for waste heat recovery. The engine achieves high efficiency as well as high reliability and low cost using low temperature heat. In addition, thermal efficiency of the engine is evaluated by experiments and the improvement of automobile fuel consumption is evaluated using a simulation model with varying engine load and exhaust gas conditions.

LIQUID-PISTON STEAM ENGINE

STRUCTURE AND PRINCIPLE OF OPERATION - Figures 1 and 2 show the schematic and the operation principle of the proposed liquid-piston steam engine. The engine is composed of heating section, cooling section to condense steam, and solid piston to extract work. The working fluid, which is water in this study, is termed “liquid piston”, because it moves in synchronization with the solid piston. The liquid water entering the heating section is vaporized to yield high pressure, which pushes the liquid surface in the downward direction. Only vaporization takes place when the vapor-liquid interface is in the heating section, because the cooling section is filled with water. After the vapor-liquid interface passes the top dead center, continuous vaporization of the remained water in the heating section maintains high pressure which further pushes down the piston. When the vapor-liquid interface is pushed down into the cooling section, steam starts to condensate. When the liquid piston is near the bottom dead center, only condensation takes place because there is no liquid left in the heating section. As the liquid piston passes the bottom dead point, the inertial energy of the flywheel pushes the piston upward to reduce the volume of the cylinder. Figure 3 illustrates an ideal cycle diagrams for the case with boiling pressure of 5 MPa and condensing pressure of 0.05 MPa.

REMARKABLE CHARACTERISTICS – Figure 4 shows comparison of *T-S* diagrams between liquid-piston steam engine and other conventional external combustion engine using Rankine or Stirling cycles. The ordinary Rankine cycle requires superheated steam in order to prevent turbine blade from corrosion, so the ideal thermal efficiency of Rankine cycle engine is inferior to that of liquid-piston steam engine under fixed temperature condition. The engine using Stirling cycle requires large temperature difference for heat exchange because working fluid is gas (in many cases its air), so the ideal thermal efficiency of Stirling cycle engine is inferior to that of liquid-piston steam engine under fixed temperature condition. Figure 5 shows the ideal thermal efficiency of these cycles against heat source temperature under the condition of condensing pressure of 0.1 MPa. For the reasons noted above, the ideal thermal efficiency of liquid-piston steam engine is superior to those of the other engines at low heat source temperature below 300 °C.

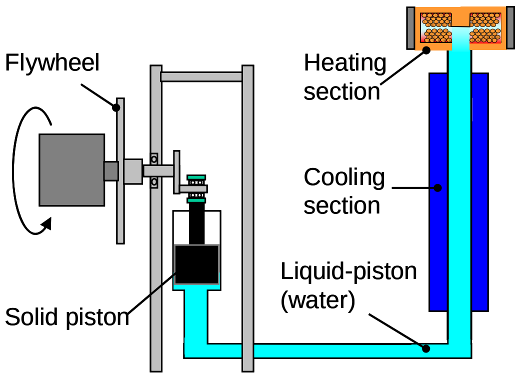

Fig. 1 Structure of liquid-piston steam engine.

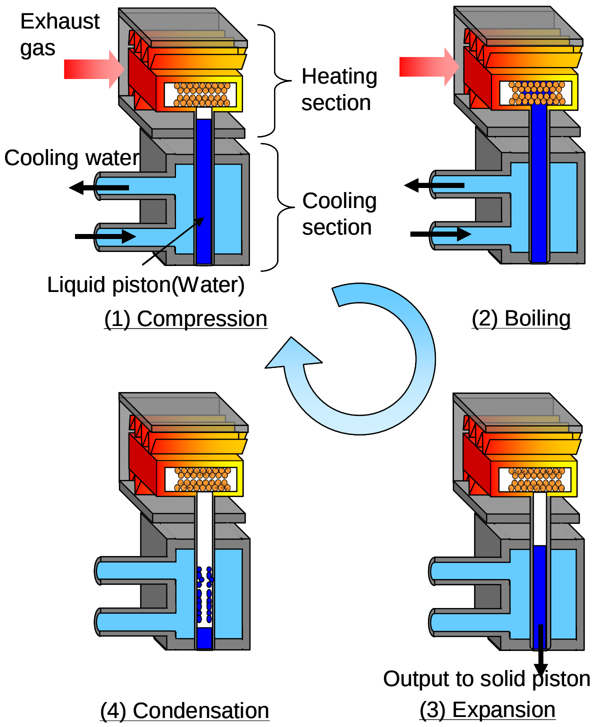

Fig. 2 Operation of liquid-piston steam engine.

A liquid-piston steam engine has only a single moving part, the solid piston, which operates at relatively low temperature. On the other hand, both Rankine and Stirling engines have at least two moving parts. In addition, the temperatures of Rankine cycle turbine or heating cylinder piston of Stirling engine are relatively high. Therefore, liquid-piston steam engine does not require relatively expensive materials and advanced technologies to achieve high reliability at high temperature. In addition, liquid-piston steam engine does not require vacuum pump because working fluid is enclosed in a sealed space and vapor is condensed to the pressure below atmospheric pressure in cooling section.

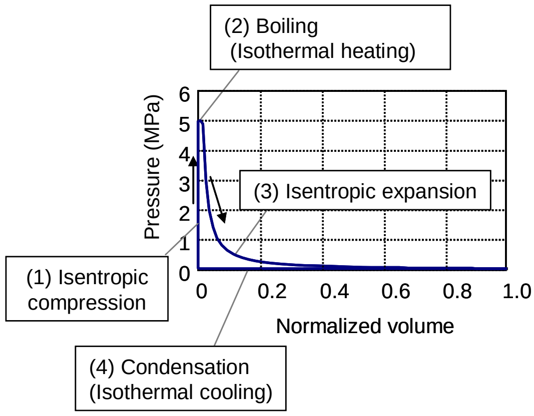

(a) *P-V* diagram

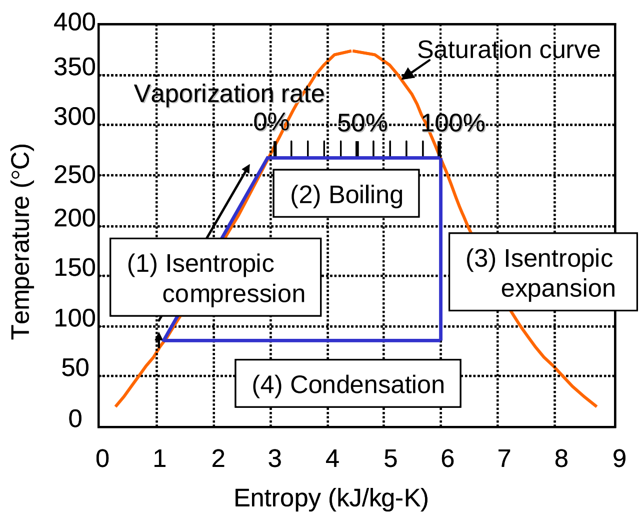

(b) *T-S* diagram

Fig. 3 Ideal cycle diagrams of liquid-piston steam engine.

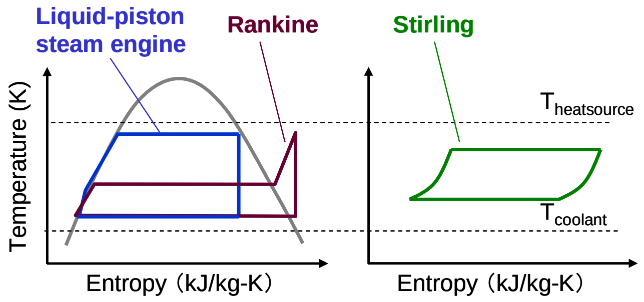

Fig. 4 *T-S* diagrams comparison between liquid-piston steam engine and other conventional external combustion engine.

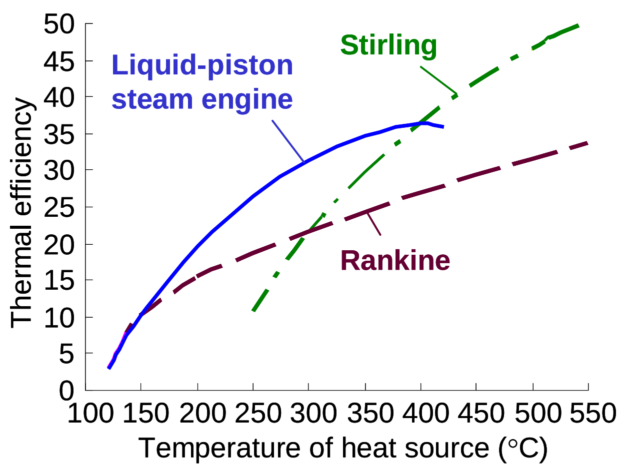

Temperature difference between temperature of heat source and high-temperature = 50°C(Liquid-piston, Rankine), 150°C(Stirling)
Low-temperature = 60°C

Fig. 5 Comparison of thermal efficiency of ideal cycle between liquid-piston steam engine, Rankine and Stirling cycles.

EXPERIMENTAL SETUP

DETAILED DESIGN OF THE HEATING SECTION - The thermal efficiency of liquid-piston steam engine was investigated experimentally. In order to design the details of the heating section, we developed a cycle simulator which calculates the thermal efficiency of liquid-piston steam engine. Figure 6 shows the flow chart of the calculation procedure. The cycle is divided into 100 intervals. The operation frequency is 3 Hz, the total stroke volume of the solid piston is 7 cc, the amount of water entering the heating section is 0.1 cc and the cooling temperature is 90 °C. Figure 7 shows the model of the heating section. The water evaporates in the cylindrical flow paths. The following assumptions are introduced in order to calculate the amount of the water evaporating at the heating section. Firstly, boiling heat flux is assumed to follow the Kutateladze's equation:

$$q(t) = 3.12\times10^{-11}\times\lambda^{3.3}\times\left(\frac{P}{\nu_L h_{fg}\rho_V\sigma}\right)^{2.3}\times\left(\frac{\sigma}{g(\rho_L-\rho_V)}\right)^{0.67}\times \mathrm{Pr}^{1.17}\times(T_W - T_s(t)),\quad (1)$$

Secondary, the boiling occurs at the saturation temperature. Thirdly, the temperature distribution of the water is calculated by the Fourier's law, and the heat flux obtained from Eq. (1) gives the wall boundary condition. Fourthly, generated steam can move to the steam reservoir immediately, which corresponds to the assumption of spatially uniform pressure in the system. Similarly, the following assumptions are introduced for condensation at the cooling section. Firstly, in expansion process, vapor condensate with constant condensation rate. Secondly, in the compression process, vapor condensates isothermally.

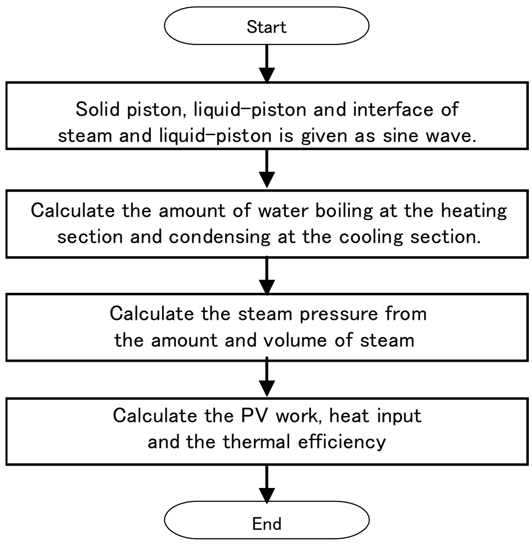

Fig. 6 Calculation procedure.

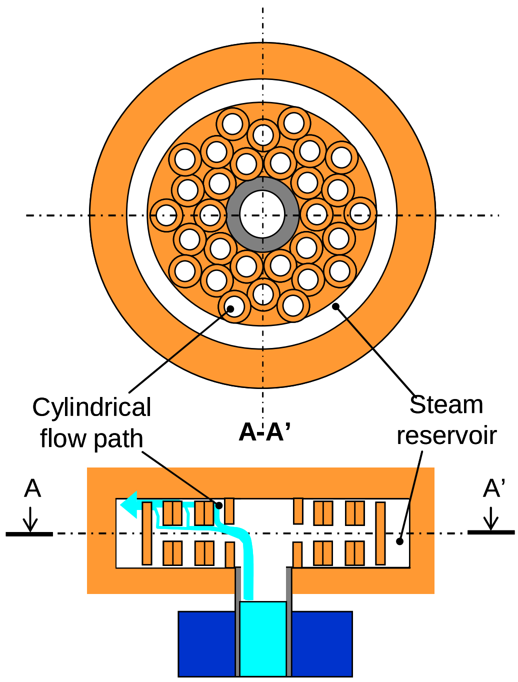

Fig. 7 Model of heating section.

Figure 8 shows the calculated thermal efficiency with different diameters of the cylindrical flow path. When the diameter becomes below 20μm, the thermal efficiency of the engine achieves 14.8% at heat source temperature of 300 °C. It is almost 50% of the ideal cycle efficiency. In order to reduce the pressure drop loss, the heating section should be designed to have small diameter and large porosity. Thus, a sintered metal heating section is developed. Figure 9 shows the structure of the sintered metal heating section. The sintered metal was molded using spark plasma sintering (SPS) method. A small pressure was applied to spherical copper granules with almost uniform diameter, which were arranged in a close-packed hexagonal lattice. Its hydraulic diameter was 23 μm and porosity was 17%. This porous structure constitutes flow paths of liquid and vapor, and at the same time works as high performance fins. The sintered metal was installed into two parallel circular copper plates. A hollow channel heating section without sintered metal was also developed for comparison.

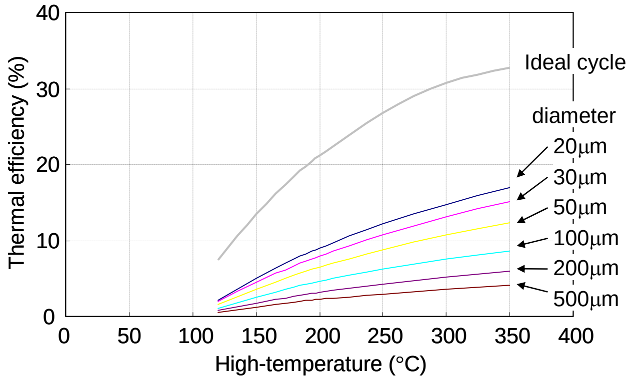

Fig. 8 Calculated thermal efficiencies against T_h with different diameter of flow path.

EXPERIMENTAL SETUP – Figure 9 shows the schematic diagram of the experimental setup. The heating section was heated by electrical band heater. Thermocouples were installed in order to measure the temperature of the heating section. Coaxial tubes are used for the cooling section. Circular SUS tube with inner diameter of 5 mm and outer diameter of 6.35 mm was used as an inner tube. The coolant water from the water chiller (SC5000a, Julabo) was circulated with inlet temperature of 80 °C. The Scotch-York mechanics converts rotating motion of the motor into reciprocating motion of the solid piston. The cycle frequency was controlled using displacement sensor signals, DSP (AutoBox and DS1103, dSPACE), DC motor and hi-speed DC amplifier. The solid piston's diameter is 20 mm and its stroke is 22 mm, so the total stroke volume is 7 cc. The stroke volume is calculated as follows:

$$V_{st} = 3.5 \times (1 - \cos\theta), \tag{2}$$

Controlling the liquid volume is very important. If the liquid temperature increases, the liquid-piston volume increases and the amount of water entering the heating section increases. As a result, more energy is consumed for vapor compression, and thus power output decreases. In contrast, when liquid-piston temperature decreases, the liquid piston volume and the amount of water entering the heat section decrease. As a result, liquid piston pressure and power output both decrease. A reserve tank and a orifice are used to control the liquid piston volume. Figure 11 shows the P-V diagrams for different volumes of the liquid piston. The pressure in the reserve tank is maintained at almost the same value as the averaged pressure of the liquid-piston under the most appropriate operating condition. With the increase of the liquid-piston volume, the averaged pressure of the liquid-piston increases, so water flow into the reserve tank through the orifice and the liquid piston volume decreases. In contrast, when the liquid-piston volume is small, the averaged pressure of the liquid piston decreases, so water flowing out from the reserve tank and the liquid-piston volume increase. Therefore, the liquid piston amount is maintained at an appropriate value.

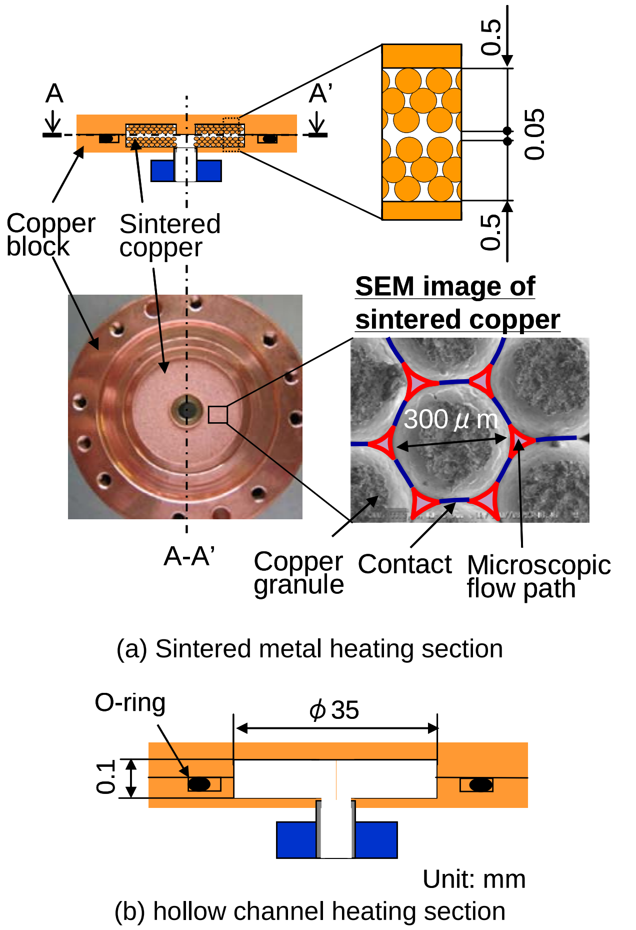

Fig. 9 Structures of the heating section.

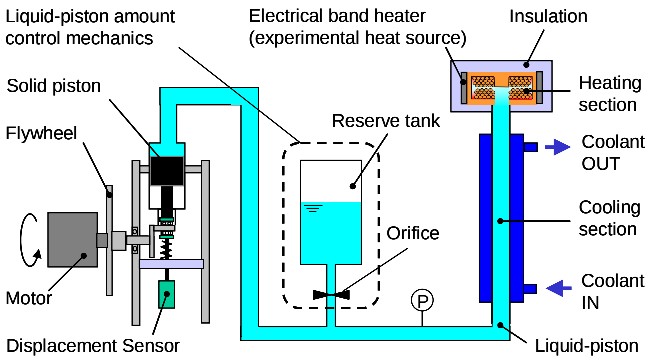

Fig. 10 Schematic diagram of the experimental setup.

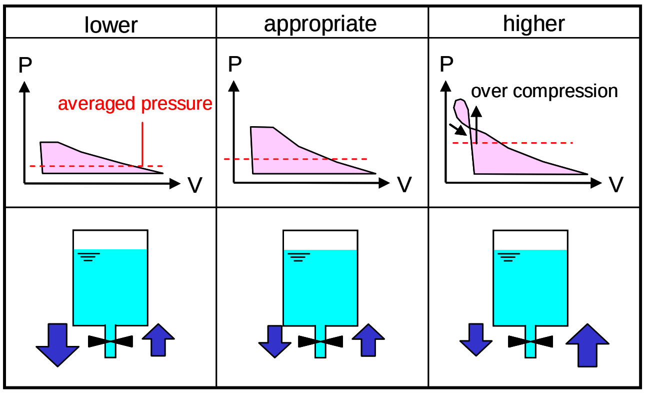

Fig. 11 PV diagrams and flow directions for different volumes of liquid piston.

EXPERIMENTAL PROCEDURE – In order to investigate the temperature dependence of the thermal efficiency, heating section temperature is controlled by varying the electrical heat input of the band heater. DC motor is used to reciprocate solid piston and liquid piston at desired frequency. *P-V* diagram is plotted using the liquid piston pressure *P* and stroke volume V_s. The amount of water entering the heating section M_{in} is detected graphically. Figure 12 shows magnified view of the measured *P-V* diagram around top dead center (TDC). When water enters the heating section, boiling occurs and operating pressure rises rapidly. So the point where operating pressure starts to rise rapidly indicates the volume and the amount of water entering the heating section. Total volume *V* is calculated as follows:

$$V = V_s + V_d \,, \tag{3}$$

Vapor temperature and entropy are calculated from *P*, *V* and M_{in} assuming saturated condition. The temperature of the heat source T_h was calculated as a maximum value of vapor temperature. *P-V* work and the thermal efficiency are calculated as follows:

$$W = \oint P dV \,, \tag{4}$$

$$\eta_{PV} = W_{PV} / Q_{hs} \tag{5}$$

$$Q_{hs} = Q_{input} + Q_{loss} \tag{6}$$

Q_{loss} was preliminarily measured experimentally.

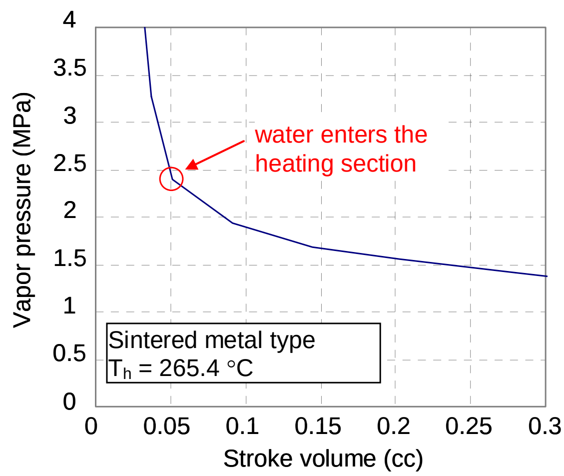

Fig. 12 Magnified view of the measured *P-V* diagram around TDC, sintered metal type, T_h = 265.4 °C.

EXPERIMENTAL RESULTS

Figure 13 shows the thermal efficiency against temperature of the heat source. Thermal efficiency increases with temperature for every heating section types. This is because vapor pressure becomes higher with the increase of temperature. Thermal efficiency of the engine with the sintered metal heating section is higher than that with the hallow channel heating section. Figure 14 shows *T-S* diagrams of the engine. It is represented that the engine with the sintered metal heating section achieves larger quality than the engine with the hollow channel heating section. In other words, the sintered metal can reduce the amount of water entering the heating section, which will contribute to reduce the sensible heat loss. In the present experiments, maximum thermal efficiency of 12.7 % at temperature of 270 °C was obtained, which was approximately 50% of the ideal cycle efficiency. Thus, liquid-piston steam engine is expected to possess large possibility for waste heat recovery.

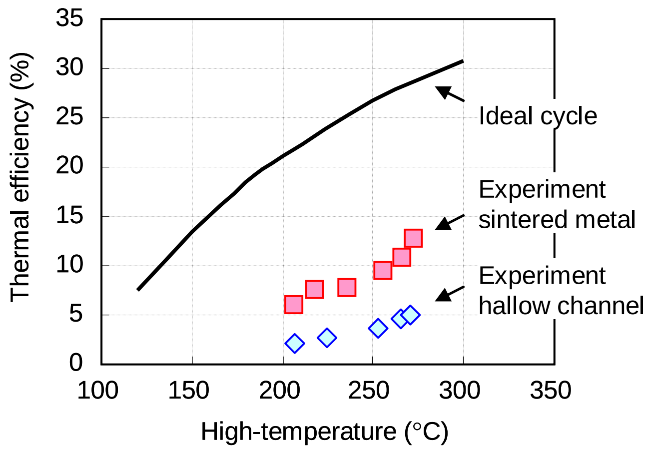

Fig. 13 Thermal efficiency against temperature.

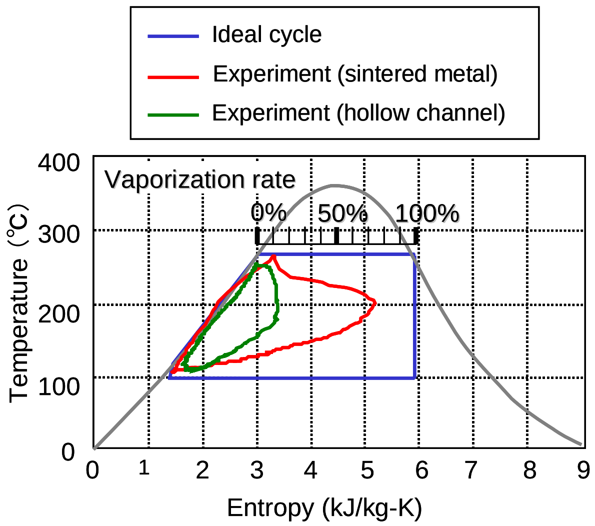

Fig. 14 *T-S* diagram of the liquid-piston steam engine.

WASTE HEAT RECOVERY SYSTEM PERFORMANCE

WASTE HEAT RECOVERY SYSTEM - In order to estimate the electrical output of the waste heat recovery system using liquid-piston steam engine, a system simulator is developed. Figure 15 shows the schematic diagram of the supposed system. Conventional gasoline engine's exhaust gas at the downstream of the catalytic module and engine cooling water are assumed as the high temperature and low temperature heat sources, respectively.. Generator converts kinetic energy into electricity and charges lead battery. The electrical output is calculated as follows:

$$W_{ele} = Q_{hs} \times \eta_{PV} \times \eta_{gen} \, , \tag{7}$$

$$Q_{hs} = m_{gas} \times Cp_{gas} \times \left(T_{gas} - T_{hs}\right) \times \eta_{ex} \, , \tag{8}$$

The temperature, the mass flow rate of exhaust gas and the thermal efficiency of the high-temperature side heat exchanger against vehicle speed were obtained experimentally. Thermal efficiency of the liquid-piston steam engine is calculated assuming that the thermal efficiency of the engine increases in proportion to the temperature of the heating section as follows:

$$\eta_{PV} = 0.000976 T_h - 0.14461 \, , \tag{9}$$

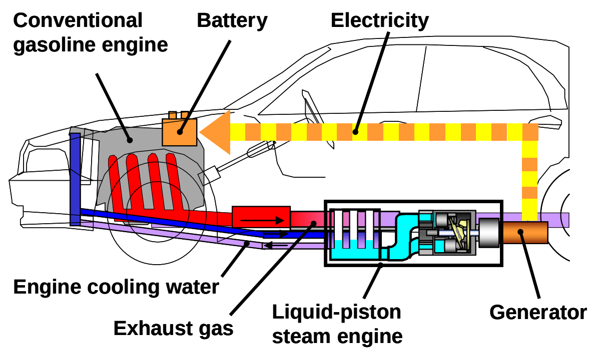

Fig. 15 Schematic diagram of waste heat recovery system for automobile exhaust gas.

SIMULATOR OUTLINES - Simulation was carried out under the assumption of New European Driving Cycle (NEDC) and Highway Fuel Economy Test (HWFET). Because of large energy variation of exhaust gas under both NEDC and HWFET, the temperature of the heating section varies largely. As a result, the thermal efficiency of the engine degrades. Thus, two kinds of operation modes are proposed. First operation mode is "heat accumulation mode" which stops the steam engine until the temperature becomes above T_{upper}. The second operation mode is "generation mode" which operates the steam engine and generates electricity using accumulated heat until the temperature becomes lower than T_{lower}. These alternative operations keep the temperature variation of the heating section moderate with higher efficiency. When the temperature of the heat section becomes higher, accumulated heat from the exhaust gas becomes smaller because of the reduced temperature difference between the heat section and the exhaust gas. We evaluated three conditions of T_{lower} and T_{upper}: (240, 270), (270, 300), (300, 330) (°C). The weight of the heat section is 6 kg and the maximum required electrical output is 400 W in view of electricity consumption of the conventional gasoline vehicle.

PERFORMANCE ESTIMATION – Figure 16 (a)-(c) show the temperature variations with time under NEDC. During most of the operation periods, temperature of the heating section is well-controlled at target temperature range. However, during the latter part which corresponds to high-speed driving, temperature exceeds the target temperature. It is suggested that the present design cannot use all of the exhaust gas energy under high-speed driving condition. Figure 17 shows the electrical output against three temperature conditions. Under NEDC, maximum output is 44 Wh at the condition of T_{lower} = 270 °C and T_{upper} = 300 °C. This amount of output is equivalent to approximately 2.7 % of the road resistance. Figure 18 shows the temperature variations with time under HWFET and Figure 19w shows the electrical output against three temperature conditions. Under HWFET, the temperature exceeds the target temperature range during most of the operation period. Maximum output is 79 Wh at the condition that T_{lower} is 300 °C and T_{upper} is 330 °C. This amount of output is equivalent to approximately 3.0 % of the road resistance. In conclusion, when the energy of exhaust gas is large, alternative operation at the high temperature condition is better.

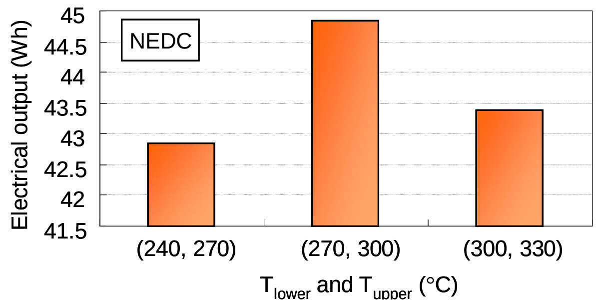

Fig. 17 Electrical output against three temperature conditions under NEDC.

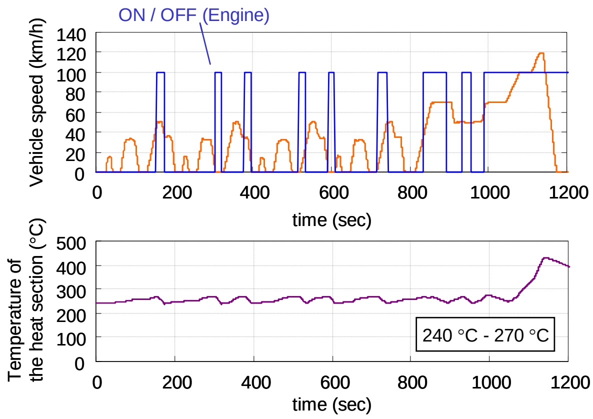

(a) T_{lower} = 240 °C, T_{upper} 270 °C.

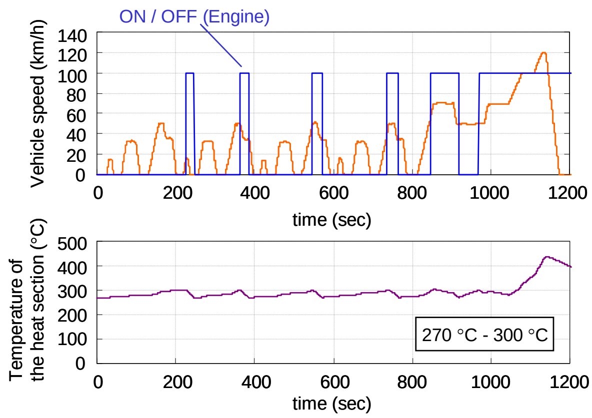

(b) T_{lower} = 270 °C, T_{upper} = 300 °C.

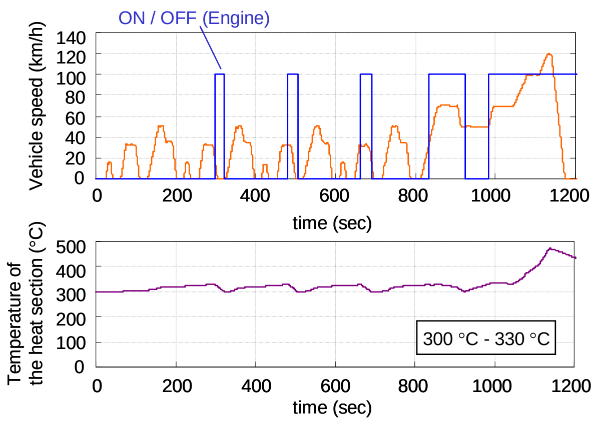

(c) T_{lower} = 300 °C, T_{upper} = 330 °C.

Fig. 16 Temperature variations with time under NEDC.

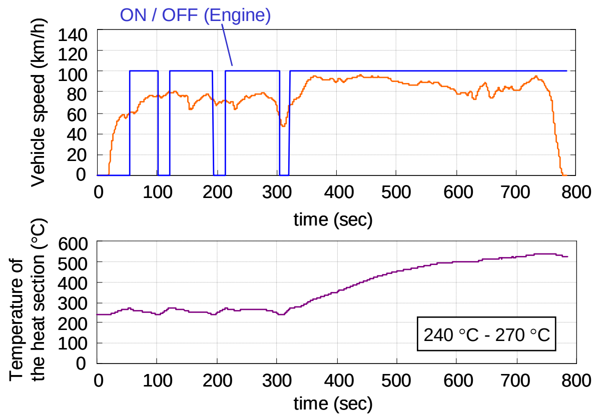

(a) T_{lower} = 240 °C, T_{upper} = 270 °C.

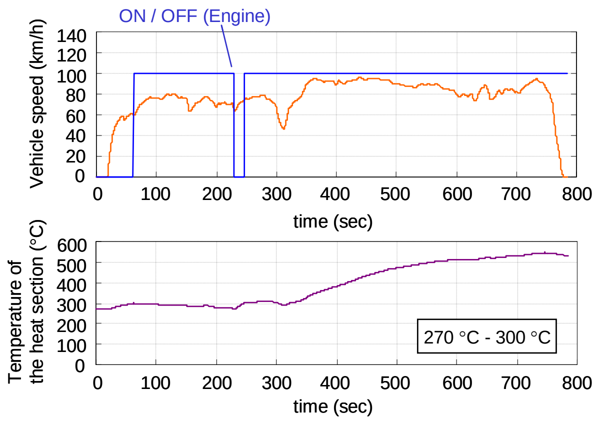

(b) T_{lower} = 270 °C, T_{upper} = 300 °C.

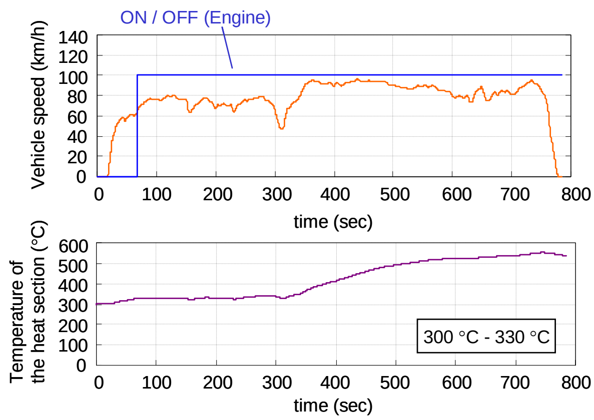

(c) T_{lower} = 300 °C, T_{upper} = 330 °C.

Fig. 18 Temperature variations with time under HWFET.

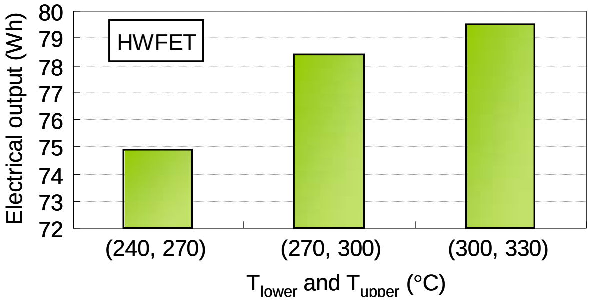

Fig. 19 Electrical output against three temperature conditions underHWFET.

CONCLUSION

A novel liquid-piston steam engine which has large potential of high efficiency, high reliability and low cost in the low temperature region is developed. Liquid piston steam engine with sintered metal heating section achieved the thermal efficiency of 12.7% at T_h = 270 °C and T_l = 80 °C. And it was demonstrated that waste heat recovery system with liquid-piston steam engine for automobile exhaust gas can generate electricity of 44 or 79 Wh under NEDC or HWFET modes, respectively.

REFERENCES

1. Wang, T., Zhang, Y., Peng, Z. and Shu, G., 2011. A review of researches on thermal exhaust heat recovery with Rankine cycle. Renewable and Sustainable Energy Reviews 15, 2862-2871.
2. Endo, T., Kawajiri, S., Kojima, Y., Takahashi, K., Baba, T., Ibaraki, S., et al., 2007. Study on maximizing exergy in automotive engines. In: SAE paper 2007-01-0257.
3. Ringler, J., Seifert, M., Guyotot, V. and Hübner, W., 2009. Rankine Cycle for Waste Heat Recovery of IC Engines. In: SAE paper 2009-01-0174.

DEFINITIONS, ACRONYMS, ABBREVIATIONS

Symbol	**Designation**
g	gravitational constant (= 9.8 m/s^2)
h	specific enthalpy (kJ/kg)
M	mass (kg)
P	pressure (MPa)
Pr	Prandtle number, Pr = $C_p\mu/\lambda$
q	heat flux (kW/m^2)
Q	heat flow (W)
t	time (s)
T	temperature (°C)
V	volume (cc)
W	output (W)
λ	thermal conductivity (W/m-K)
ν	kinematic viscosity (Pa-s)
σ	surface tension (N/m)
η	thermal efficiency
θ	phase angle (°), TDC: 0°, BDC: 180°

ABBREVIATIONS	**Designation**
cs	cool source
d	dead volume
ele	electricity
ex	high-temperature side heat exchanger
fg	latent heat
gas	exhaust gas
gen	convert P-V work into electricity
h	high-temperature side of cycle
hs	heat source
in	enter in the heating section
input	electrical heater input
l	low-temperature side of cycle
loss	heat dissipation from outer surface of the heating section
lower	lower limit of controlled temperature
L	liquid
PV	P-V work
s	saturated
st	stroke
t	total
upper	upper limit of controlled temperature
V	vapor
w	wall